Robotica (2022), **40**, pp. 1450–1474
doi:10.1017/S0263574721001211

CAMBRIDGE
UNIVERSITY PRESS

RESEARCH ARTICLE

An energy efficiency index for elastic actuators during resonant motion

Andrea Calanca[1,*] and Tom Verstraten[2]

[1]Department of Computer Science, University of Verona - Verona, Italy and [2]Robotics and Multibody Mechanics Research Group (R&MM), Vrije Universiteit Brussel/Flanders Make - Brussels, Belgium
*Corresponding author. E-mail: andrea.calanca@gmail.com

Received: 13 January 2021; **Revised:** 28 July 2021; **Accepted:** 3 August 2021; **First published online:** 4 October 2021

Keywords: Energy Efficiency; Power Consumption; Series Elastic Actuators; Parallel Elastic Actuators; Passive Dynamics

Abstract

The energetic advantages of series and parallel elastic actuators have been characterized in the literature considering different elastic systems and different tasks. These characterizations usually determine the energy consumption of a specific system during a specific task and generalize poorly. This paper proposes an energetic characterization of elastic actuators, following an analytical approach, rather than a data-driven one. In particular, this work analyzes the energy consumption of elastic actuators during resonant motion and introduces a novel efficiency index. This index characterizes energy consumption as a function of inherent actuator parameters only, generalizing over the specific tasks. The proposed analysis is validated using simulations and experiments, demonstrating its coherence with analytical results.

1. Introduction

Mechanical compliance is one of the main enabling factors of animal efficient locomotion. Muscles and tendons exhibit inherent elasticity, which allows to reduce the energy consumption by storing and releasing potential elastic energy [1–3]. Today, elastic components are widely used also in robotic research, fostered by introduction of elastic actuation technology [4]. While the original motivation for introducing (series) elasticity was to ease the difficult force control of stiff actuators [5–10], it soon became evident that elastic components also provide high efficiency in resonant motions [11–15] and help to reduce the size and weight of drivetrains and their power supply systems [16–19]. Robotic locomotion represents a relevant example where energy efficiency can be improved by elastic energy storage. Passive and quasi-passive dynamic walkers often incorporate series and parallel elastic components to recover the negative work or to store the ground impact energy. Some of these advantages can be explained using the spring-loaded inverted pendulum (SLIP) model [20] where terminal springs make the ground impact elastic, thus preserving the system's internal energy. In contrast, in a rigid locomotion model – such as the compass model [21] – the impact is inelastic and impulsive, thus a part of the internal energy is dissipated at each cycle. For these reasons, modern legged robots and lower limbs orthoses and prostheses often include elastic components by design [22–27]. Another application where power consumption could be reduced by exploiting elasticity is represented by repetitive factory operations such as pick-and-place tasks, as experimentally shown in refs. [28, 29]. In spite of these documented advantages, a generic analytical characterization of robot efficiency in such applications is missing. This is most likely due to the nonlinear and multidimensional nature of the considered systems, which makes the analytical efficiency characterization very complex.

A further advantage of passive elastic dynamics is that motion may naturally arise from the inherent system "morphology" (i.e. the system dynamics/kinematics) without the need for a traditional motion

© The Author(s), 2021. Published by Cambridge University Press.

https://doi.org/10.1017/S0263574721001211 Published online by Cambridge University Press

control system.[1] The term "morphological computation" captures a paradigm shift where the control algorithm provides only the necessary input power to let a *resonant motion* arise from the inherent system morphology.[2]

Let us take the example of an ideal PDW with elastic impacts. During locomotion, the walker exhibits a constant level of internal energy, which leads it to produce natural motion. In the real world, there will be some dissipation, which needs to be compensated to perpetuate the motion. This can be done by one or more actuators that produce a driving force (torque) at the natural frequency, giving rise to resonant motion. In general, the dissipation level depends on both inherent system properties (e.g. damping) and the specific motion (e.g. different locomotion velocities imply different levels of dissipation). In this paper, we are interested in understanding which system properties affect the energetics of resonant motion, in order to design efficient passive dynamic systems. However, due to the complexity of the analysis and because the energetics of complex robotic systems are defined by the energetics of simpler subsystems, this paper focuses on minimal subsystems capable of energy storage and analyzes the energy consumption of series and parallel elastic actuators (SEAs and PEAs) in resonant motions. Focusing on passive-dynamic applications, we introduce an efficiency index η that characterizes the tendency of a passive system to perpetuate its natural motion. In particular, the specific contributions are

1. a novel energetic characterization of elastic actuators accounting for the system internal energy that gives rise to the resonant motion;
2. an efficiency index η that uses internal energy to normalize across different motion "magnitudes";
3. the derivation of this index for the specific cases of SEA and PEA as a function of actuator's mechanical properties;
4. the insight that the energy stored in the system's nonresonant modes is related to higher energy consumption; this finding has never been reported before.

As the existing literature on elastic actuator efficiency is still quite empirical and system-specific, a main objective of this work is to show the viability of an analytical approach that can be used to gain a more general knowledge. To focus on the methodology framework while keeping the argumentation simpler, this paper does not address the combination of multiple SEAs and PEAs and the analysis is restricted to the mechanical domain. Extensions to multiple d.o.f. and the inclusion of the electrical dynamics will be the subject of future research.

Finally, we emphasize that this work only discuses efficiency at system resonance. In other words, although our analysis generalizes over the amplitude of the motion, it assumes that the system is designed to work at a particular frequency – the resonance frequency. This is often the case in morphological computation or in efficient locomotion applications. It must be noted that, if the system's dynamics change over time, the selected spring stiffness may become inadequate and the efficiency of the system may drop drastically [14]. For this reason, variable stiffness actuators have been introduced, which allow to adapt the spring's stiffness to the task [30].

The paper is organized as follows. Literature on elastic actuator efficiency is summarized in Section 2 where we also introduce our approach. Section 3 proposes an energetic characterization of systems in resonant motion that motivates and defines our methodology. Such methodology is applied to the cases of parallel and series elastic actuators (SEA) in Sections 4 and 5, respectively, and a discussion

[1] A traditional motion control system is responsible for computing and imposing the desired motion to the robot leading to stiff controlled systems with high power demand. In other words, a traditional motion control system uses energy to stiffen the robot dynamics in order to obtain precise motion tracking.

[2] Different kinds of morphological computation systems exist. In some cases, the actuator acts as a motion source and the inherent system kinematics "processes" the motion. In other examples, the actuator acts as an energy source and the inherent system dynamics "processes" the energy. We are interested in the latter class of systems (which includes passive dynamic walkers (PDWs)) and we use the term morphological computation to refer to this type of systems.

https://doi.org/10.1017/S0263574721001211 Published online by Cambridge University Press

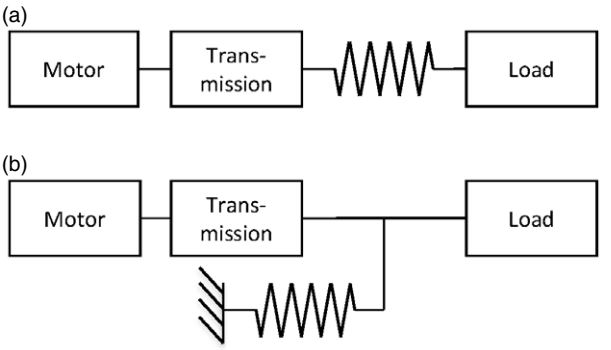


Figure 1. *Schematic representation of the two main elastic actuator architectures: (a) SEA, (b) PEA.*

of analytical results is reported in Section 6. Simulations and experimental validations are reported in Section 7. Finally, conclusions are drawn in Section 8.

2. Background and Proposed Approach

2.1. Elastic actuators

Elastic actuators are typically classified in two main types, depending on the placement of the elastic element [19]. A schematic of these two architectures can be found in Fig. 1. In SEA, the elastic element is placed between the drivetrain and the load, that is, in a series configuration. Another option is to place the elastic element in parallel with the drivetrain, resulting in a parallel elastic actuator (PEA). It is widely known that both architectures can generate energy-efficient cyclic motion if a (roughly) linear relationship exists between the required output torque and the output angle. This, for example, applies to resonant motion. Both architectures take advantage of the possibility of recirculating power between the motor, the spring and the load, an option which is unavailable in rigid actuators. In the latter, power often travels back and forth through the actuator, resulting in the accumulation of losses in its components [31]. Recirculating power between the spring and the load has two advantages. First, power losses – which are more or less proportional to the power flowing through the actuator – are reduced. Second, the reduced power demand can often be met with a smaller electric motor and gearbox, which drives down the size, weight, and cost of the actuation system [19].

The mechanism by which the required motor power is reduced differs between the two architectures. In a well-designed PEA, the parallel spring will take over part of the load torque, resulting in a decrease of the torque required from the motor [18]. The motor will, however, rotate at the same speed as the output, since it is directly coupled to the latter. In contrast, a well-designed SEA will allow to reduce the required motor speed below that of the output. A SEA can, however, not compensate for a static load [15], although reductions in motor torque can be achieved in dynamic motions because of the reduced acceleration of the drivetrain, which is associated with a decrease in inertial torque. As we will discuss extensively in this manuscript, these characteristic differences between SEA and PEA will result in different efficiencies for resonant motions.

2.2. Energetic characterization

Several papers analyzed the energetic advantages of elastic actuators. Rather than being based on an analytical approach, most of these analyses are data driven. They typically consider a specific system and experimentally measure the forces and velocities needed for a specific task. Then, they simulate and optimize the properties of elastic elements so that the actuators produce the same force/velocity profiles with (hopefully) reduced power consumption. The advantage of this methodology is that it can be applied to a great variety of systems and tasks. On the other hand, the results are task specific and sensitive to

https://doi.org/10.1017/S0263574721001211 Published online by Cambridge University Press

experimental conditions, in the sense that the analysis must be repeated from scratch when changes are made to the task or to the new system. This approach is followed in several papers on exoskeletons [24, 32–34] and powered prostheses [19, 35–38], where authors optimize elastic components in series or parallel to different human joints, taking gait data as a starting point for the kinematics. These results are task specific, since they depend on the locomotion speed. Several other examples of system-specific and task-specific analyses can be found, for example, on walking robots [25, 39–41], hopping robots [42–44], manipulators [45–48] and even wheeled robots [49]. In search of generalized rules for elastic actuator design, some authors have studied the motion of a pendulum at different frequencies. In [50, 51] the efficiency of several variable stiffness actuators is compared in simulation and in [13, 50] the efficiency of series and parallel elastic actuators is compared in simulation and real-world experiments.

In all the aforementioned works, the energy efficiency is expressed in terms of energy or power costs, in a form similar to

$$\eta_1 = \frac{1}{input\ power} \tag{1}$$

which is task specific. The literature usually considers nonlinear and multi degree of freedom systems for which an analytical efficiency analysis is extremely challenging. The only analytical analysis found in literature [12] considers a simpler system (a SEA) and uses the traditional efficiency index

$$\eta_2 = \frac{output\ power}{input\ power}. \tag{2}$$

This index assumes that work is done on the environment; if not, the efficiency goes to zero. Thus, experiments in ref. [12] are carried out by coupling the actuator with a dissipative environment and measuring the output work. Quite surprisingly, the outcome of their work is that the maximum efficiency increases with environmental damping. This can be explained by the fact that the energy is mainly dissipated by something that is considered external to the system while a minor amount of energy is dissipated internally.

Another common efficiency index in locomotion is the cost of transport (COT), which is defined as

$$COT = \frac{input\ power}{weight \times velocity}. \tag{3}$$

The COT is a nondimensional quantity and represents a ratio between the cost (input power) and the benefit (transported weight at a given speed) of a transportation mode [51, 52]. Similarly to other approaches, the *COT* is task-specific as it depends on the specific transportation velocity.

In conclusion, the existing efficiency analyses are empirical, that is, driven by simulation or experimental data rather than by analytical computations. Moreover, most of the indices found in the literature are task specific as they evaluate the efficiency of a system given a certain task: η_1 can only be used to compare efficiency within identical tasks while the *COT* depends on the transportation velocity. The only exception is the index η_2 which, however, implies that the environment dissipation improves efficiency. These indices are not representative of the concept of efficiency as it is intended in this work.

2.3. Proposed approach

In general, energy efficiency is related to the amount of input power that is wasted when completing a certain job or task. In this paper, we are interested in the task of maintaining a resonant motion. Here, efficiency regards the input power needed to support such a motion. To evaluate this scenario, we introduce a novel index η which indicates "how fast" the internal energy is dissipated during a resonant motion. In particular, η relates the system's internal energy to the mean input power needed to support the resonant motion:

$$\eta = \frac{internal\ energy}{mean\ input\ power}. \tag{4}$$

https://doi.org/10.1017/S0263574721001211 Published online by Cambridge University Press

The index η is expressed in time units and characterizes the tendency of a passive system to perpetuate its natural motion. For the moment we can assume that the input power is equal to the dissipated power.[3] The index η can roughly be interpreted as the duration of the natural motion when no external power is supplied. A low value for η means that little motion can be observed before the system dissipates all its internal energy. Vice-versa, a high η means long-lasting motion. The index η ranges between $[0, +\infty)$, where 0 implies no observable natural motion (no internal energy storage) while $+\infty$ corresponds to perpetual natural motion (no dissipation). Alternatively, the index η can be interpreted as a measure of power consumption (denominator) with a normalization factor (numerator), eliminating the effect of the natural motion "magnitude." In fact, different motion "magnitudes" involve different levels of internal energy, which in turn involve different dissipation levels.

3. Resonant Motion Energetics

For a generic electromechanical system, the power balance can be written as

$$input\ power = \frac{dE}{dt} + dissipation + output\ power \tag{5}$$

where E is the system's internal energy, which may give rise to resonant motion. After transients, the internal energy stored in the system continuously alternates between kinetic and potential energy, with a rhythm given by the system's natural frequencies. To support the motion (to maintain the internal energy level), the dissipated power and output power (if any) need to be compensated by a corresponding input power.

Before proceeding, we point out that while the "shape" of the resonant motion mainly depends on the system dynamics (e.g. a linear dynamics may give rise to sinusoidal motion), the magnitude mainly depends on the quantity of involved energy. We used the term "mainly" because in the case of nonlinear systems the "shape" is also affected by the internal energy level. Moreover, in high-order systems the "shape" also depends on initial conditions which define the distribution of the initial energy within the system modes. In this paper, we limit the analysis to linear systems of elastic actuators, where the natural motion is always sinusoidal.

As a first observation it is important to highlight that the energy E stored within a system can be of two kinds. The first is the energy which is involved in the resonant modes, and which continuously alternates between kinetic and potential. In this work, this energy is called *resonant energy* and is referred as E_r. The second is a kind of energy which is present within the system but cannot be permanently stored in resonant modes; it just temporarily flows though the system. We will call it *temporary energy* using the symbol E_t. The temporary energy arises because a system may exhibit different modes (e.g. resonances) which can only store energy when excited at their natural frequency, otherwise the energy just flows though these modes without being stored (the term "stored" can be equivalently interpreted as "accumulated"). Let us consider the example of an electromagnetic motor (without any springs attached) and let us apply a sinusoidal current to it. When the rotor is accelerating we have positive input power as well as an increase of rotor kinetic energy. When the rotor is decelerating (the current is braking the rotor), the kinetic energy is converted into negative input power which flows back to the driver. This happens because the motor alone cannot store energy supplied with sinusoidal excitation. The energy just temporarily flows into the system and then exits as negative input power. If instead a spring is attached in series with the motor and we apply a sinusoidal current at the resonance frequency, we would observe energy accumulating in the resonance mode, resonant energy. However, if we excite the system with different frequencies, we would observe again energy coming back to the driver as negative input power.

[3] Some hypotheses should be considered here, which are detailed in the next section.

https://doi.org/10.1017/S0263574721001211 Published online by Cambridge University Press

Remark 1. As the overall system internal energy is the sum of resonant and temporary energy, $E = E_r + E_t$, Eq. (5) can be rewritten as

$$input\ power = \frac{dE_r}{dt} + \frac{dE_t}{dt} + dissipation + output\ power. \tag{6}$$

Remark 2. When the system is in steady state, it is storing all the resonant energy to perform the task, we are in the condition $\frac{dE_r}{dt} \approx 0$ and Eq. (6) simplifies to

$$input\ power = \frac{dE_t}{dt} + dissipation + output\ power. \tag{7}$$

Remark 3. Since "morphological computation" is usually understood as achieving resonant motion without performing work on the environment, Eq. (6) can be often simplified as

$$input\ power = \frac{dE_t}{dt} + dissipation. \tag{8}$$

Both Eqs. (7) and (8) indicate that *the variation of temporary energy affects energy consumption* as more input power is required. Thus,

Remark 4. The increase of temporary energy can be related to energy dissipation. More specifically, the temporary energy can give rise to the following additional types of dissipation:

- *Type A dissipation* due to unrecovered negative input power; this power, described by the term $\frac{dE_t}{dt}$, enters the system, is temporarily stored, and then comes back to the motor driver where it is dissipated;
- *Type B dissipation* arising within the nonresonant modes; these are parasitic dissipations within the system caused by the additional flow of temporary energy;

Type *A* dissipation arises in the case of negative input power (e.g. when the current is braking the rotor) and in the absence of an energy recovery system on the motor driver, which could recycle the braking energy. Indeed, unless an energy recovery circuit is used, the braking energy is dissipated by electrical resistors on the driver. The dissipation of type *B* arises because, being stored as kinetic energy, the temporary energy causes additional motion (involving nonresonant modes) which in turn causes additional dissipation. If we neglect the dissipation of type *B*, the same amount of supplied power comes back to the power supply system, where it can be recovered or dissipated.

If we completely neglect the effects of temporary energy, the input power P_{in} is solely used to compensate for dissipation within the resonant modes, thus $\bar{P}_{in} = \bar{P}_{dis,r}$, where $\bar{P}_{dis,r}$ is the mean power dissipated within the resonant modes, and the index (4) can be computed as

$$\eta = \frac{E_r}{\bar{P}_{dis,r}} \tag{9}$$

where E_r is the resonant energy, stored in resonant modes. Instead, if we consider the effects of temporary energy, the input power is used to compensate for dissipation within resonant modes and nonresonant modes (type *B* dissipation), and to compensate for the temporary energy dissipated by the driver (type *A* dissipation). In particular, the input power flowing from the driver will supply for the dissipated and temporary energy. The index accounting for the dissipation due to temporary energy can then be computed as

$$\eta^{TE} = \frac{E_r}{\bar{P}_{dis,r} + \bar{P}_{dis,tA} + \bar{P}_{dis,tB}} \tag{10}$$

where, $\bar{P}_{dis,r}$ is the power dissipated within resonant modes, $\bar{P}_{dis,tB}$ is the power dissipated within nonresonant modes and $\bar{P}_{dis,tA}$ is the negative input power dissipated within the driver. Unfortunately, the temporary energy is difficult to quantify as it may depend on load dynamics, as will be explained further ahead. However, it is possible to consider the worst case condition, the load or environment dynamics leading to the maximum temporary energy and compute the worst case index

https://doi.org/10.1017/S0263574721001211 Published online by Cambridge University Press

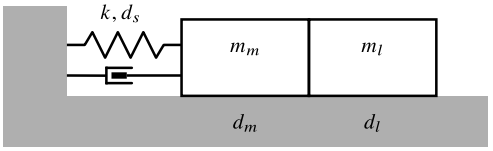


Figure 2. *A representation of a PEA coupled with an inertial load.*

$$\eta^{WC} = \frac{E_r}{\bar{P}_{dis,r} + \bar{P}^{WC}_{dis,tA} + \bar{P}^{WC}_{dis,tB}} \tag{11}$$

where $\bar{P}^{WC}_{dis,tA}$ and $\bar{P}^{WC}_{dis,tB}$ are the worst case version of $\bar{P}_{dis,tA}$ and $\bar{P}_{dis,tB}$, respectively. Of course we have $\eta \geq \eta^{TE} \geq \eta^{WC}$, the efficiency of the real system η^{TE} lies between the value η which completely neglects temporary energy, and the value η^{WC} which accounts for the maximum amount of temporary energy.

Accounting for all these considerations, the index η and the worst case index η^{WC} are computed as described in the following steps. Considering a given mechanical system,

1. modal analysis is used to separate resonant and nonresonant modes (if any) which are related to resonant and temporary energy, respectively;
2. we choose initial conditions corresponding to a certain resonant energy level E_r, design a dissipation compensation law to maintain this initial energy level E_r, and compute the associated mean dissipated power $\bar{P}_{dis,r}$;
3. we compute $\eta = E_r/\bar{P}_{dis,r}$, which (as shown in the following section) cancels out the motion magnitude, causing η to depend only on actuator parameters and not on the particular motion; this index is related to the case of *temporary energy recovery* and neglects dissipation in nonresonant modes, the temporary energy is not accounted for;
4. we compute the worst case index η^{WC} which accounts for the highest *temporary energy* within the system.

In the following Sections 4 and 5, this procedure is applied to the cases of parallel and SEA.

4. Analysis of Parallel Elastic Actuators

PEAs often consist of electromagnetic motors which have their stator fixed to ground and their rotor connected to a spring, with the opposite end of the spring connected to the ground [14, 15]. The rotor is also rigidly connected to a link or to a load as represented in Fig. 2 where angular variables are converted into linear equivalents. The mass m_m represents the rotor inertia, m_l is the link, and k is the spring stiffness. Dissipation sources may be located between the rotor and stator, such as the damping due to bearings or brushes, in parallel to the spring, due to non ideal elastic behavior and on the load, representing dissipations due to the environment. These dissipation sources are characterized here by the damping coefficients d_m, d_s and d_l. The motor transmission is considered fully backdrivable. The notation used in this section and in the following is summarized in Table I. Defining $M = m_m + m_l$ and $D = d_m + d_s + d_l$, the system dynamics can be expressed as

$$M\ddot{x}_l(t) + D\dot{x}_l(t) + kx_l(t) = F(t). \tag{12}$$

where x_l is the load position. It follows that the input that exactly compensates for dissipation is $F(t) = D\dot{x}_l(t)$. By applying this input and by choosing initial conditions $x_l(0) = 0$ and $\dot{x}_l(0) = \alpha\omega_P$, where $\omega_P = \sqrt{\frac{k}{M}}$ is the resonance frequency of the PEA, we have the following state trajectories

$$x_l(t) = \alpha \sin(\omega_P t) \tag{13a}$$

https://doi.org/10.1017/S0263574721001211 Published online by Cambridge University Press

Table I. *System parameters.*

Parameter	Symbol	Parameter	Symbol
Motor inertia	m_m	Spring stiffness	k
Load inertia	m_l	Motor damping	d_m
Quantity μ	$\mu = m_l/m_m$	Spring Damping	d_s
Quantity m	$m = 1 + \mu$	Load Damping	d_l
PEA Resonance		$\omega_S^2 = \frac{k}{m_m + m_l}$	
SEA Resonance		$\omega_S^2 = k\left(\frac{1}{m_m} + \frac{1}{m_l}\right) = \frac{km}{m_l}$	

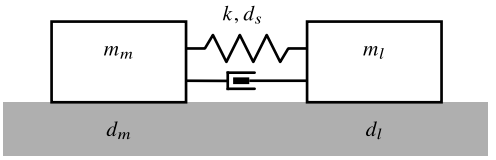


Figure 3. *A representation of a SEA coupled with an inertial load.*

$$\dot{x}_l(t) = \alpha\omega_S \cos(\omega_P t) \tag{13b}$$

which describes a resonant motion. Thus, the system (12) oscillates at its natural frequency with constant resonant energy E_r

$$E_r = K + U = \frac{1}{2}M\dot{x}_l(t)^2 + \frac{1}{2}kx_l(t)^2 = \frac{1}{2}k\alpha^2 \tag{14}$$

where K and U are kinetic and potential energy. The dissipated power is $P_{dis} = D\dot{x}_l^2(t)$ which can be averaged over the period $T = 2\pi/\omega_S$ leading to

$$\bar{P}_{dis,r} = \frac{1}{T}\int_0^T D\dot{x}_l^2(t)dt = \frac{Dk\alpha^2}{2M} \tag{15}$$

where $\dot{x}_l$ has been substituted as in (13b). Then, we can compute the index η as

$$\eta = \frac{E_r}{\bar{P}_{dis,r}} = \frac{M}{D} = \frac{m_m + m_l}{d_m + d_s + d_l}. \tag{16}$$

We observe from (16) that the motion magnitude α is canceled out, as anticipated in the previous section. As the PEA model (12) is second order, it exhibits a single (resonant) mode. Consequently, all the internal energy is stored in this resonant mode and no temporary energy is present in the system. In this case

$$\eta = \eta^{TE} = \eta^{WC}. \tag{17}$$

5. Analysis of Series Elastic Actuators

In typical SEA architectures, the stator of the motor is fixed to ground and the rotor is connected to the link or to the load by means of an elastic element. This is represented in Fig. 3 where, again, angular variables are converted into linear equivalents. The mass m_m represents the rotor inertia with position x_m and m_l is the link or load inertia with position x_l. The elastic element in between is characterized by stiffness k and damping d_s and the motor transmission is considered fully backdrivable. Other dissipation sources are located between the rotor and stator (d_m) and on the load (d_l). The resulting system dynamics are

$$m_m\ddot{x}_m = F - d_m\dot{x}_m - k(x_m - x_l) - d_s(\dot{x}_m - \dot{x}_l) \tag{18a}$$

https://doi.org/10.1017/S0263574721001211 Published online by Cambridge University Press

$$m_l\ddot{x}_l = -d_l\dot{x}_l + k(x_m - x_l) + d_s(\dot{x}_m - \dot{x}_l) \tag{18b}$$

where x_m is the motor position, x_l is the load position and time dependency of $x_m(t)$, $x_l(t)$ and $F(t)$ is omitted for space reasons. The SEA model (18a)-(18b) is fourth order which, in modal coordinates, results in one oscillatory mode and one translatory mode.[4] Consequently, when the system is excited at its natural frequency, the oscillatory mode stores the resonant energy while some temporary energy may flow in the translatory mode. In contrast to PEAs, damping parameters cannot be aggregated and each dissipation source is analyzed separately in the following sections.

5.1. Motor damping

Similarly to the case of PEA, motor damping can be compensated by positing $F(t) = d_m\dot{x}_m(t)$ which leads to the following system dynamics

$$m_m\ddot{x}_m(t) = -k(x_m(t) - x_l(t)) \tag{19a}$$

$$m_l\ddot{x}_l(t) = k(x_m(t) - x_l(t)) \tag{19b}$$

which exhibits a resonant frequency in

$$\omega_S = \sqrt{\frac{k}{m_m} + \frac{k}{m_l}}. \tag{20}$$

In order to observe the system during a resonant motion, we consider the initial conditions $x_m(0) = x_l(0) = 0$, $\dot{x}_m(0) = \alpha\omega_S\mu$ and $\dot{x}_l(0) = -\alpha\omega_S$ leading to the following motion equations

$$x_m(t) = -\mu\alpha \sin(\omega_S t) \tag{21}$$

$$\dot{x}_m(t) = -\mu\alpha\omega_S \cos(\omega_S t) \tag{22}$$

$$x_l(t) = \alpha \sin(\omega_S t) \tag{23}$$

$$\dot{x}_l(t) = \alpha\omega_S \cos(\omega_S t) \tag{24}$$

where $\mu = m_l/m_m$. The internal energy can be computed by considering

$$K = \frac{1}{2}m_m\dot{x}_m^2 + \frac{1}{2}m_l\dot{x}_l^2 = \frac{1}{2}\alpha^2\omega_S^2 m_l(1+\mu)\cos^2\omega_S t \tag{25}$$

$$U = \frac{1}{2}k(x_m - x_l)^2 = \frac{1}{2}\alpha^2 k(1+\mu)^2 \sin^2\omega_S t \tag{26}$$

which leads to

$$E = U + K = \frac{1}{2}\alpha^2 k(1+\mu)^2. \tag{27}$$

Thus, the total internal energy E is constant over time and is completely stored in the resonant mode. As a consequence, no temporary energy arises.[5] The mean dissipated power for damping compensation can be expressed as

$$\bar{P}_{d_m} = d_m \frac{1}{T}\int_0^T \dot{x}_m^2(t)dt \tag{28}$$

[4] According to modal analysis, a system mode involves a second-order differential equation which corresponds to a couple of states in the sense of system theory. The term translatory mode is used here to refer to integrator-like dynamics which give rise to in-phase oscillations of masses m_m and m_l.

[5] This can also be shown by expressing the SEA model (18a)-(18b) in modal coordinates, similarly to the approach followed in the next section.

https://doi.org/10.1017/S0263574721001211 Published online by Cambridge University Press

where $T = 2\pi/\omega_S$. Considering that $\frac{1}{T}\int_0^T \sin^2 \omega_S t = \frac{1}{2}$, we have

$$\bar{P}_{d_m} = \frac{1}{2} d_m \mu^2 \alpha^2 \omega_S^2 = \frac{1}{2} \alpha^2 k \frac{\mu(1+\mu)}{m_m} d_m \tag{29}$$

and we can finally compute the index

$$\eta_m = \frac{E_r}{\bar{P}_{d_m}} = \frac{m_m + m_l}{d_m} \frac{m_m}{m_l}. \tag{30}$$

5.2. Spring damping

When the damping is located in the spring, it is convenient to explicitly distinguish between the resonant and the translatory modes. To this aim, the SEA model (18a)-(18b) can be expressed in modal coordinates as

$$z_1 = m^{-1}(\mu x_l + x_m) \tag{31a}$$

$$z_2 = m^{-1}(x_l - x_m) \tag{31b}$$

where $m = 1 + \mu$, leading to the modal representation

$$M_p \begin{bmatrix} \ddot{z}_1 \\ \ddot{z}_2 \end{bmatrix} + D_p \begin{bmatrix} \dot{z}_1 \\ \dot{z}_2 \end{bmatrix} + K_p \begin{bmatrix} z_1 \\ z_2 \end{bmatrix} = \begin{bmatrix} F \\ -\mu F \end{bmatrix} \tag{32}$$

where

$$M_p = \begin{bmatrix} m m_m & 0 \\ 0 & m m_l \end{bmatrix}, \tag{33a}$$

$$D_p = \begin{bmatrix} d_m + d_l & d_l - \mu d_m \\ d_l - \mu d_m & m^2 d_s + \mu^2 d_m + d_l \end{bmatrix}, \tag{33b}$$

$$K_p = \begin{bmatrix} 0 & 0 \\ 0 & m^2 k \end{bmatrix}. \tag{33c}$$

Here the states z_1 and $\dot{z}_1$ describe the translatory mode while z_2 and $\dot{z}_2$ represent the resonant mode. The modal transformation (31a)-(31b) is energy preserving and allows to easily distinguish the resonant energy, stored in states z_2 and $\dot{z}_2$, from the temporary energy, stored in states z_1 and $\dot{z}_1$.

If we consider a single dissipation source given by d_s, the damping matrix D_p is diagonal and the Eqs. (32) become decoupled:

$$m m_m \ddot{z}_1 = F \tag{34a}$$

$$m m_l \ddot{z}_2 + m^2 d_s \dot{z}_2 + m^2 k z = -\mu F. \tag{34b}$$

Focusing on the latter row we can impose

$$F = -\frac{m^2}{\mu} d_s \dot{z}_2 = \frac{1+\mu}{\mu}(x_m - x_l) \tag{35}$$

to have perfect damping compensation. Similarly as before, initial conditions can be chosen on order to observe the following resonant motion

$$z_2(t) = \alpha \sin(\omega_S t) \tag{36}$$

$$\dot{z}_2(t) = \alpha \omega_S \cos(\omega_S t) \tag{37}$$

https://doi.org/10.1017/S0263574721001211 Published online by Cambridge University Press

which implies a constant level of resonant energy

$$E_r = K_2 + U_2 = \frac{1}{2} m m_l \dot{z}_2^2 + \frac{1}{2} m^2 k z^2 = \frac{1}{2} \alpha^2 m^2 k. \tag{38}$$

The average power needed for damping compensation can be computed from (35) as

$$\bar{P}_{d_s,r} = m^2 d_s \frac{1}{T} \int_0^T \dot{z}_2^2(t) dt = \frac{1}{2} \alpha^2 m^3 k \frac{d_s}{m_l} \tag{39}$$

and finally we have

$$\eta_s = \frac{E_r}{\bar{P}_{d_s}} = \frac{m_l}{m d_s} = \frac{m_m m_l}{m_m + m_l} \frac{1}{d_s}. \tag{40}$$

5.2.1. Accounting for Temporary Energy

By substituting (35) in (34a) we find that, in order to compensate for d_s, some energy is introduced in the mode z_1 leading the two masses to oscillate in-phase. Unfortunately, the system cannot permanently store this energy because, as reported in (34a) the mode z_1 exhibits pure integrator dynamics. The temporary energy is just temporarily stored in the state $\dot{z}_1$ as kinetic energy and then exits the system as negative input power. In particular, given the input (35) and a proper choice of initial conditions, we can solve Eq. (34a) and compute

$$\dot{z}_1 = -\alpha \frac{m}{m_l} d_s \sin \omega_S t. \tag{41}$$

The associated kinetic energy is

$$K_1 = \frac{1}{2} m m_m \dot{z}_1^2 = \frac{1}{2} \alpha^2 \frac{m^3}{\mu m_l} d_s^2 \sin^2 \omega_S t \tag{42}$$

which increases in the first quarter of the period and decreases in the second quarter. In a half period ($T/2$) such temporary energy is released as negative input power which may be dissipated by the motor driver. Such dissipated power can be computed by relating the released energy with the releasing period $T/2$ leading to

$$\bar{P}^{WC}_{d_s,tA} = \frac{\max(K_1)}{T/2} = f \alpha^2 \frac{m^3}{\mu m_l} d_s^2 \tag{43}$$

where $f = 1/T = \omega_S/2\pi$ is the resonance frequency of the SEA and ω_S is defined in (20). It is worth highlighting that such dissipated power is related to worst case condition. Indeed, the amount of temporary energy is reduced when the load inertia m_l is constrained by some downstream dynamics. For example, in the limit case of fixed load inertia there will be no temporary energy because no in-phase oscillation can occur. In contrast, when the load mass is completely unconstrained, we have the highest temporary energy and higher associated dissipated power which represents the worst case condition (WC) for efficiency. The worst case index can be computed considering such worst case dissipated power as

$$\eta_s^{WC} = \frac{E_r}{\bar{P}^{WC}_{d_s,tA}} = \frac{\eta_s}{1 + \frac{f d_s}{\mu k}} \tag{44}$$

or equivalently as

$$\eta_s^{WC} = \frac{\eta_s}{1 + \sigma d_s}, \quad \sigma = \frac{m_m}{m_l \sqrt{k \cdot m_m || m_l}} \tag{45}$$

where the notation $m_m \parallel m_l$ indicates the parallel of motor and load inertias $m_m \parallel m_l = \frac{m_m m_l}{m_m + m_l}$. This index accounts for dissipation of type A, while dissipation of type B is not observed because no dissipation term related to state $\dot{z}_1$ exists in Eqs. (34a)-(34b). By looking at the coefficient σ it seems that such dissipation (type A) increases when the motor inertia is high and at the same time the load inertia is

https://doi.org/10.1017/S0263574721001211 Published online by Cambridge University Press

low. Also, it decreases with the actuator stiffness. Thus, rigid systems which avoid the combination of high motor inertia and lightweight load seem to be more efficient in the sense that they are less prone to dissipation due to the temporary energy.

5.3. Load damping

In the case of load damping we can consider the following modal equations

$$mm_m\ddot{z}_1 + d_l\dot{z}_1 + d_l\dot{z}_2 = F \tag{46a}$$

$$mm_l\ddot{z}_2 + d_l\dot{z}_1 + d_l\dot{z}_2 + m^2kz_2 = -\mu F \tag{46b}$$

with states $\dot{z}_2,\ z_2$ representing the oscillatory mode and $\dot{z}_1,\ z_1$ the translatory mode. In this case both system modes are involved in energy dissipation, leading to type *B* dissipation. Focusing on (46b), damping terms can be compensated by imposing $F = -\frac{d_l}{\mu}(\dot{z}_1 + \dot{z}_2) = -\frac{d_l}{\mu}\dot{x}_l$ which lets the system oscillate at its natural frequency. The system dynamics then becomes

$$m_m\ddot{z}_1 + d_l\dot{z}_1 + d_l\dot{z}_2 = 0 \tag{47a}$$

$$m_l\ddot{z}_2 + mkz_2 = 0. \tag{47b}$$

Similarly to previous sections, initial conditions can be chosen on order to observe the following resonant motion

$$z_2(t) = \alpha \sin(\omega_S t) \tag{48a}$$

$$\dot{z}_2(t) = \alpha\omega_S \cos(\omega_S t). \tag{48b}$$

The resonant energy is stored in the states $\dot{z}_2,\ z_2$ and can be computed as in the previous section

$$E_r = \frac{1}{2}\alpha^2 m^2 k. \tag{49}$$

If we neglect the temporary energy by considering $z_1 = \dot{z}_1 = 0$, the average dissipated power is

$$\bar{P}_{d_l,r} = d_l\frac{1}{T}\int_0^T \dot{z}_2^2(t)dt = \frac{1}{2}\alpha^2\omega_S^2 d_L \tag{50}$$

and the index η_l can be expressed as

$$\eta_l = \frac{E_r}{\bar{P}_{d_l,r}} = \frac{m_m + m_l}{d_l}\frac{m_m}{m_l}. \tag{51}$$

5.3.1. Accounting for Temporary Energy

When compensating for load damping, we have dissipation of both type *A* and *B*. The first is due to the temporary energy exiting the system as negative input power (and then being dissipated by the motor driver). The second is due to the dissipative terms $d_l\dot{z}_1$ in (46a) and (46b). As before, to characterize the worst case dissipation, the trajectory of z_1 is computed by considering an unconstrained load. In particular, Eq. (47a) can be solved in the Laplace domain by replacing z_2 with its transform leading to

$$z_1(s) = \frac{-\alpha\gamma\omega_S}{(s+\gamma)(s^2+\omega_S^2)} \tag{52}$$

where $\gamma = \frac{d_l}{m_l}$. Then by anti-transformation and proper choice of initial conditions it is possible to express z_1 as

$$z_1(t) = \frac{-\alpha}{\gamma^2+\omega_S^2}(\gamma\omega_S e^{-\gamma t} + \gamma\omega_S \cos\omega_S t + \gamma^2 \sin\omega_S t). \tag{53}$$

https://doi.org/10.1017/S0263574721001211 Published online by Cambridge University Press

The exponential term just represents a transient and is neglected from here on. The power within system modes can be computed as $P_{d_l} + P_{d_l}^{WC-B} = d_l(\dot{z}_1 + \dot{z}_2)^2$. It also accounts for type B dissipation due to the worst case temporary energy. The trajectory $\dot{z}_1$ can be derived from (53) as

$$\dot{z}_1(t) = \frac{\alpha}{\gamma^2 + \omega_S^2}(\gamma^2 \omega_S \cos \omega_S t - \gamma \omega_S^2 \sin \omega_S t) \tag{54}$$

while $\dot{z}_2$ is expressed in (48b). By defining $h = \frac{\omega_S^2}{\gamma^2} = \frac{kmm_l}{d_l^2}$, the dissipated power can be computed as

$$P_{d_l,r} + P_{d_l,tB}^{WC} = d_l \alpha^2 \left(\frac{h+2}{h+1} \omega_S \cos \omega_S t - \frac{h}{h+1} \gamma \sin \omega_S t \right)^2 \tag{55}$$

and on average we have

$$P_{d_l,r} + P_{d_l,tB}^{WC} = \frac{1}{2} \alpha^2 \omega_S^2 (1 + 3\xi) d_l \tag{56}$$

where $\xi = \frac{1}{h+1}$. The efficiency index accounting for worst case type B dissipations can be computed as

$$\eta_l^{WC-B} = \frac{E_r}{P_{d_l,r} + P_{d_l,tB}^{WC}} = \frac{m_m + m_l}{d_l} \frac{m_m}{m_l} \frac{1}{(1 + 3\xi)}. \tag{57}$$

Again, this index is worst case because the load mass is unconstrained, leading to the maximum temporary energy flowing into the system (maximum in-phase oscillations). As we are not yet accounting for type A dissipations, η_l^{WC-B} describes the case of a system capable of recovering the negative input power. We can say that a SEA with an energy recovery circuit can exhibit an efficiency index with a value between η_l in (51), where the temporary energy was entirely neglected, and η_l^{WC-B} in (57), depending on the load/environment dynamics. Interestingly, the ratio between η_l and η_l^{WC-B} is given by the coefficient $\frac{1}{(1+3\xi)}$ which can reduce the worst case efficiency by no more than a quarter. Indeed, since $h > 0$, one has that $0 \leq \xi \leq 1$. When k is high the quantity ξ is small and we again find that a series elastic system with high stiffness leads to higher efficiency in resonant motions, because the temporary energy flow is minimized. A similar effect can be observed for high load and low motor inertia.

Finally, to compute type A dissipation we need to consider the negative input power dissipated by the motor driver in absence of an energy recovery circuit. As in previous section $\bar{P}_{d_l,tA}^{WC}$ is given by the kinetic energy which is temporarily stored in the state $\dot{z}_1$ and then released

$$K_1 = \frac{1}{2} m m_m \dot{z}_1^2 \tag{58a}$$

$$= \frac{1}{2} m m_m \alpha \omega^2 \left[\frac{1}{h+1} \cos \omega_S t - \frac{h}{h+1} \sin \omega_S t) \right]^2. \tag{58b}$$

The negative input power can be computed as before considering the amount of released energy max (K_1) within the releasing period $T/2$. After some small computations[6] this leads to

$$\bar{P}_{d_l,tA}^{WC} = \frac{\max(K_1)}{T/2} = \frac{1}{2} \alpha^2 f \frac{m m_m}{m_2} d_l^2 (1 - \xi) \tag{59}$$

[6]We considered the trigonometric equation $\max([\frac{1}{h+1} \cos \omega_S t - \frac{h}{h+1} \sin \omega_S t)]^2) = [(\frac{1}{h+1})^2 + (\frac{h}{h+1})^2]$.

https://doi.org/10.1017/S0263574721001211 Published online by Cambridge University Press

Table II. *Overview of Computed Indices*

	PEA	SEA
η_m	$\frac{m_m+m_l}{d_m}$	$\frac{m_m+m_l}{d_m}\ \frac{m_m}{m_l}$
η_s	$\frac{m_m+m_l}{d_s}$	$\frac{m_m \Vert m_l}{d_s}$
η_l	$\frac{m_m+m_l}{d_l}$	$\frac{m_m+m_l}{d_l}\ \frac{m_l}{m_m}$

Table III. *Correction Terms due to Temporary Energy*

	SEA
η_s^{WC-B}	η_s
η_s^{WC}	$\frac{\eta_s}{1+\sigma d_s}$
η_l^{WC-B}	$\frac{\eta_l}{(1+3\xi)},\ 0 \le \xi \le 1$
η_l^{WC}	$\frac{\eta_l}{1+3\xi+\sigma(1-\xi)d_l}$

and the worst case efficiency index in absence of an energy recovery circuit is

$$\eta_l^{WC} = \frac{E_r}{P_{d_l,r} + P_{d_l,tB}^{WC} + P_{d_l,tA}^{WC}} \tag{60a}$$

$$= \frac{\eta_l}{1 + \sigma d_l(1-\xi) + 3\xi}. \tag{60b}$$

Interestingly, when $\xi = 0$ Eq. (60a) reduces to the following expression

$$\eta_l^{WC} = \frac{\eta_l}{1 + \sigma d_l} \tag{61}$$

which is similar to the case of spring damping (45).

6. Discussion of Analytical Results

To summarize our findings, Table II reports the index η for PEAs and SEAs, distinguishing the cases of motor, spring and load dissipation. These expressions completely neglect the temporary energy, possibly leading to an overestimation of η_s and η_l in the SEA case. Table III reports the associated correction terms when accounting for the maximum (worst case) flux of temporary energy, arising when the load inertia is unconstrained. Indices η_s^{WC} and η_l^{WC} consider a scenario of temporary energy dissipation within motor drivers, while η_s^{WC-B} and η_l^{WC-B} consider the availability of an energy recovery circuit, thus they only account for type B dissipation. In the case of spring damping, type B dissipation does not occur, thus $\eta_s^{WC-B} = \eta_s$. In this case, once the temporary energy is recovered, its net contribution is becomes null. The same does not hold in the case of load damping.

The overall energy consumption arising from the combination of different sources can be computed by simply adding the related "inefficiencies" as

$$\frac{1}{\eta} = \frac{1}{\eta_m} + \frac{1}{\eta_s^*} + \frac{1}{\eta_l^*} \tag{62}$$

where the apex $*$ means that, depending on the scenario, the terms in Table III can be used instead of the ones in Table II. Equation (62) can easily be derived considering that all the indices in Tables III and II share the same numerator, E_r.

We observe that all the indices reported in Table II are proportional to inertial quantities and inversely proportional to damping parameters. Given the same damping, the larger the inertia is, the more the system is inclined to preserve internal energy and its resonant motion as a consequence. Returning to the

https://doi.org/10.1017/S0263574721001211 Published online by Cambridge University Press

example of PDWs, a walker with high inertia is expected to exhibit longer lasting motion with respect to a lighter one, thanks to its higher kinetic energy storage capabilities (assuming similar damping coefficients for both walkers). A second observation is that the index η (4) can be related to the COT (3) to define the efficiency of a transportation task. In particular, if we consider the transportation of a load with mass m and damping d, we have

$$COT = \frac{dv^2}{mgv} \tag{63}$$

where v is the transportation velocity. Such an inertial system with mass m and damping d can be modeled as a second-order system with a pure integrator. The index η as defined in (4) can then be computed following the methodology described in Section 3, resulting in $\eta = m/d$. In this case the system exhibits a single translatory mode which represents the "resonant" mode[7] and the velocity v represents the amplitude of the translatory motion. Thus, we have

$$COT = \frac{v}{\eta g}$$

where we can distinguish system-related parameters, m and d, both embedded in η, the task-related parameter v, and the constant g. As stated in Section I, η describes the system efficiency in terms of system parameters and independently from the specific task characterized by v. Thus, disregarding the task, the system efficiency (or inefficiency) expressed by the COT can be equivalently expressed using the proposed index η. This finding supports the general validity of our analysis.

7. Validation

To validate the consistency of the proposed analysis and the accuracy of the indices in Tables II and III, we compare them with energy consumption measures in a simulation scenario and validate them in a physical environment.

7.1. Simulation Validation

In our simulations, we consider a scenario where the load is unconstrained (maximum temporary energy) and no energy recovery circuit is available. This can be considered as a worst case scenario for the SEA, because in several applications the load is somehow constrained. For example, if we consider a legged robot with the robot's foot as a load, we find that the foot is constrained to the ground during the stance phase, and it is constrained by gravity forces during other phases. Similarly, if we consider pick-and-place applications, dynamic constraints due to gravity apply. A set of inertial ($m_m,\ m_l$) and damping ($d_m,\ d_s,\ d_l$) parameters are considered while the spring stiffness (k) is fixed. The set of inertial parameters ranges from $10^{-4}\ Kgm^2$ to $1\ Kgm^2$ and includes typical values of rotor reflected inertias, representative of a wide set of electromagnetic gear-motors, from direct-drive to high gear-ratio. Similarly, we impose realistic damping values in the range of $(10^{-3}, 10^{-2})\ Nm/rad$. The stiffness parameter is set to $k = 100\ Nm/rad$ and represents a typical choice for SEAs whose stiffness ranges from some tens to some hundreds of Nm/rad. We chose to fix this value as the efficiency index η do not depend on k, as reported in Table II

The following damping compensation laws are implemented

$$F_{PEA} = (d_m + d_s + d_l)\,\dot{x}_l(t) \tag{64}$$

$$F_{SEA} = \left(d_m + \frac{1+\mu}{\mu} d_l\right)\dot{x}_m(t) - \left(\frac{1+\mu}{\mu} d_s + \frac{1}{\mu} d_l\right)\dot{x}_l(t) \tag{65}$$

for the case of PEA and SEA, as derived in the analysis in sections 4 and 5.

[7] A pure integrator exhibits infinite amplitude at zero-frequency which could be interpreted as a particular resonance frequency: the kinetic energy of a translatory motion can be indeed stored in such mode.

https://doi.org/10.1017/S0263574721001211 Published online by Cambridge University Press

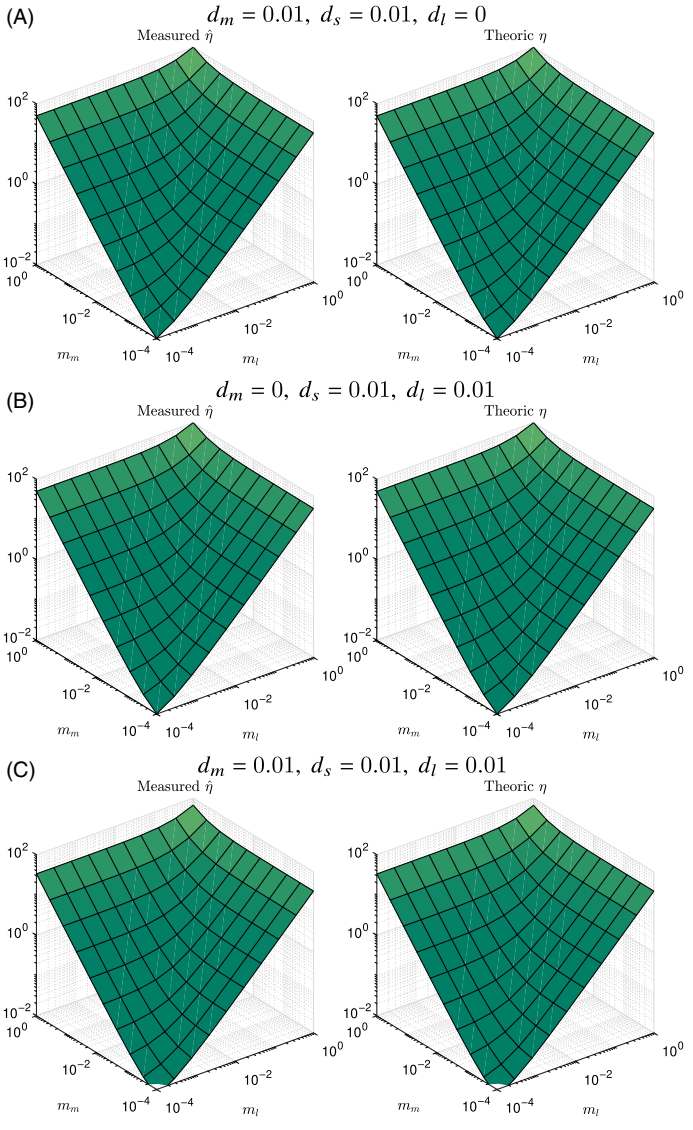


Figure 4. *Comparison between measured (left) and analytical (right) efficiency indices for PEAs.*

Efficiency is measured according to (9) as

$$\hat{\eta} = E_r / mean(P_{in}^{+}(t)) \tag{66}$$

where P_{in}^{+} represents the power flowing from the driver to the motor (which is dissipated in the mechanical domain) plus the power flowing back from the motor to the driver (which is dissipated within the motor driver, as a recovery circuit is not included). More specifically, $P_{in}^{+}(t)$ is computed as the absolute value $P_{in}^{+}(t) = |\dot{x}_m(t)F(t)|$ where $\dot{x}_m$ and F represent the motor velocity and the motor input force or torque, proportional to the current.

Figure 4 shows, for the case of PEA, the measured index $\hat{\eta}$ against the index η analytically computed as in Table II. One can observe that measured and theoretic plots present the same shape. The maximum relative error between the two is quantified as 0.264%. Logarithmic scales on the X and Y axes are chosen in order to span very different values of m_m and m_l. Similarly, we choose logarithmic scales on the Z axis in order to highlight differences between measured and theoretic indices, as the efficiency indices span very different magnitudes. Figure 5 shows the same results for the case of SEA. Here the

https://doi.org/10.1017/S0263574721001211 Published online by Cambridge University Press

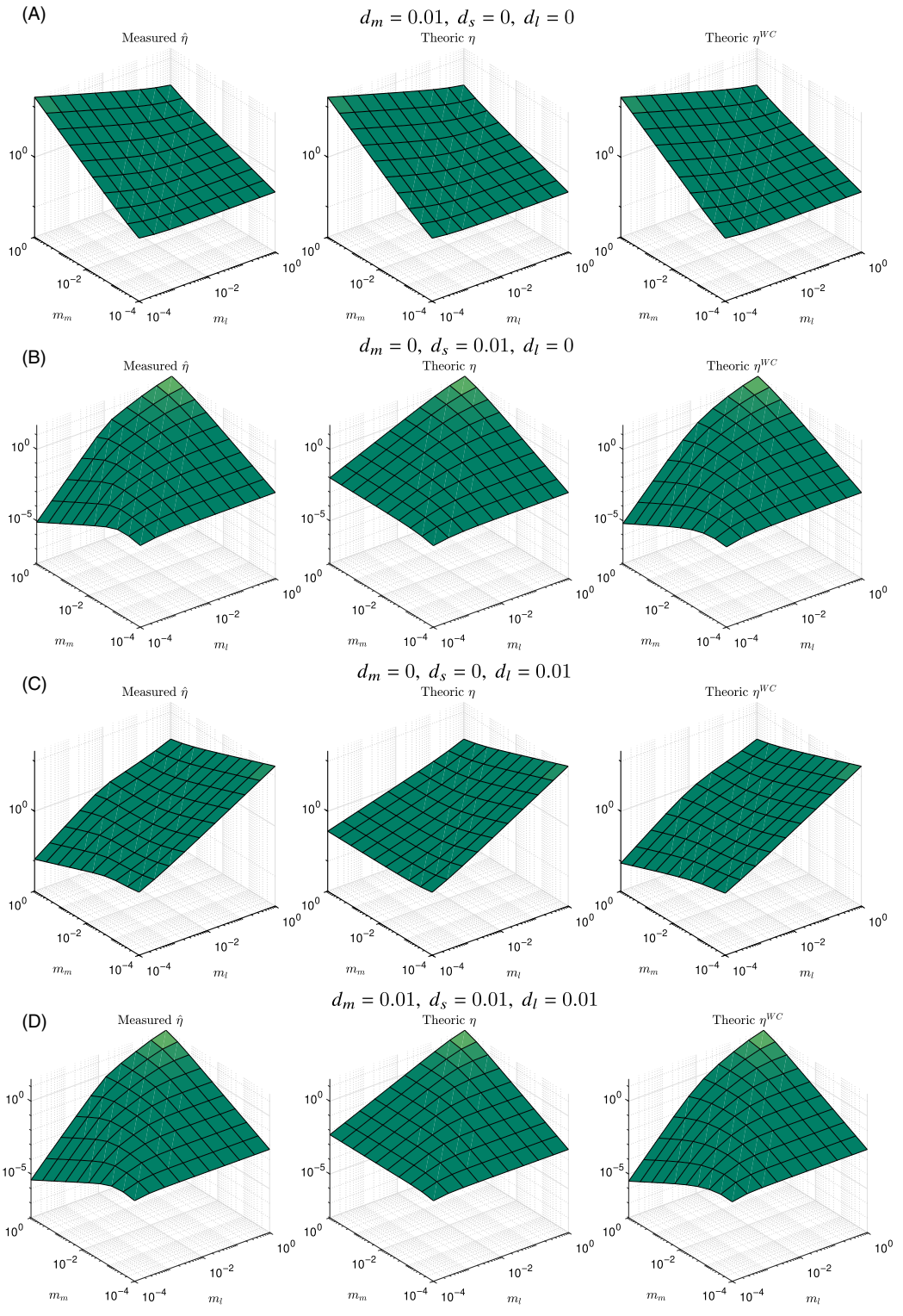


Figure 5. *Comparison between measured (left column) and theoretic indices for SEAs.*

https://doi.org/10.1017/S0263574721001211 Published online by Cambridge University Press

measured values are compared with the proposed indices, either accounting or not accounting for the effects of temporary energy. As expected, the measured efficiency presents the same shape of the worst case index η^{WC}. This is not because the index η^{WC} is more accurate, but because we simulated worst case scenarios (maximum temporary energy). We highlight that on a linear scale the discrepancy of indices η and η^{WC} would be not significant, as we show here after. Nevertheless, the proposed indices are able to capture even small differences and show consistency with measured efficiency even on a logarithmic scale. We can conclude that, both for PEA and SEA, the measured efficiency agrees with our theoretical expectations, thus validating our theoretical analysis.

Before proceeding, we highlight some particularities regarding the case of SEA. First, the difference between indices η and η^{WC} on a linear scale is extremely small. To make it noticeable, we needed to apply an extremely low value for the stiffness $k = 1\ Nm/rad$ – outside of the typical stiffness value ranges for SEA designs – and high distal friction values. These results are reported in Figure 6, where a linear scale is used for the Y axis. In these plots, we avoid showing the measured efficiency as it would overlap with η^{WC} (as reported in Figure 5). Three different values are considered for m_m and two for k. Even if η and η^{WC} are very close to each other, some differences can be observed in case of high distal friction. This agrees with the equations reported in Table III. Also, by comparing the first three rows A1, A2, and A3 – where we considered a stiffness $k = 100\ Nm/rad$ – with the last three rows B1, B2 and B3 – where we considered a very low stiffness $k = 1\ Nm/rad$ – one can observe that η^{WC} decreases, leading to more noticeable differences. This is because η^{WC} depends on σ and ξ which in turns depends on k. Instead, η does not change with k as reported in Table II. Thus, if we neglect the (small) temporary energy dissipation, we can state that k affects the resonance frequency location, but not the efficiency magnitude. Finally, we highlight that even if the plots reported in Figure 5 for the SEA show a maximum discrepancy between η and η^{WC} for high m_m and low m_l, this is not a general result. This is just due to the combination of two choices: the considered parameter set and the logarithmic scale, as can be observed by comparing Figures 5 and 6.

7.2. Experimental Validation

In the previous section, an extensive validation has been provided in simulation, considering a wide set of inertia parameters. Since it is not practically feasible to test many mechanical arrangements in experiments, we choose to experimentally validate the few scenarios representing the more complex conditions highlighted by the proposed methodology. In particular, this section proposes an experimental validation considering the case of a SEA with different lightweight loads. The experimental setup consists of the elastic actuator prototype in figure 7. It is composed of a direct drive torque motor M connected in series to a spring S (used in torsional mode) and to an exchangeable load L. System parameters have been estimated using a procedure similar to the one described in ref. [53] and are reported in Table IV, where m_{li} for $i = 1...4$ refers to different load inertias. As the inherent mechanical damping is low, we used a soft spring in order to obtain noticeably differences between indices η and η^{WC} as discussed in the previous section. For each load, Table III reports the parameters ξ and σ defined in (56) and (45). The motor Coulomb friction is compensated using a sign($\dot{x}_m$) function and neglected because its nonlinear nature is not considered in our analysis. Static and stick-slip friction are not compensated because of their complex dynamics.

Two optical encoders $E1$ and $E2$ are used to measure motor and load position, respectively. They are connected to an industrial rack that drives a motor current amplifier and provides an EtherCat connection to a standard PC on which the control algorithm runs. No energy recovery system is present in the motor driver.

In our analysis, we assume the resonant energy is maintained by perfect damping compensation. However, it is very challenging to obtain perfect damping compensation in the real world. Static and stick-slip friction dynamics are hard to model and estimation of system parameter may suffer some bias. Thus, in practice, friction and damping forces will always be either overestimated or underestimated, resulting in either an increase or a decrease in the initial system energy. To keep the internal energy

https://doi.org/10.1017/S0263574721001211 Published online by Cambridge University Press

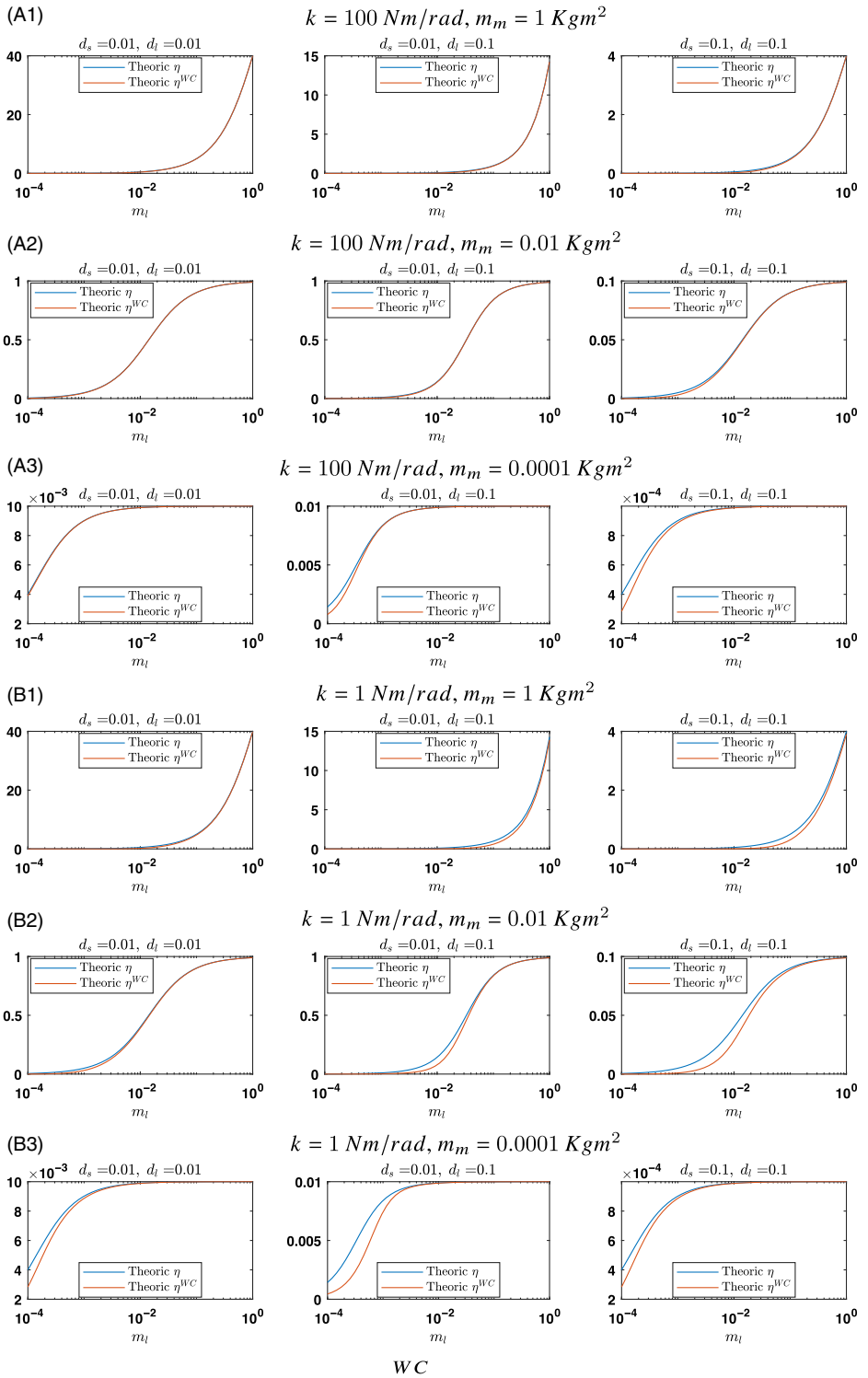


Figure 6. *Comparison between indices η and η^{WC} on linear scales, for SEAs with increasing values of parameters d_s and d_l and for different values of m_m.*

https://doi.org/10.1017/S0263574721001211 Published online by Cambridge University Press

Table IV. *Parameters of the Experimental Setup*

Parameter	**Symbol**	**Value**		
Spring Stiffness	k	$1.040\ Nm/rad$		
Torque constant	k_t	$0.42\ Nm/A$		
Motor inertia	m_m	$0.00041\ kg/m^2$		
Motor Damping	d_m	$\simeq 0.002 Nms$		
Spring Damping	d_s	$\simeq 0.0001 Nms$		
Load Damping	d_l	$\simeq 0.003 Nms$	σ	ξ
Load Inertia 1	m_{l1}	$0.00068\ kg/m^2$	37.0	0.995
Load Inertia 2	m_{l2}	$0.0099\ kg/m^2$	2.05	~ 1
Load Inertia 3	m_{l3}	$0.0307\ kg/m^2$	0.65	~ 1
Load Inertia 4	m_{l4}	$0.0868\ kg/m^2$	0.23	~ 1

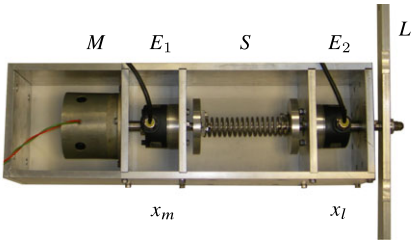


Figure 7. *The SEA prototype used as testbed.*

constant, we therefore relied on an energy-based control approach. Energy control injects power into the system until a desired level E_d of internal energy E is reached. This strategy has been used for example to control PDWs [54]. According to [54] energy control can be formulated as

$$F(t) = k_e(E_d - E(t))\dot{x}_m(t) \tag{67}$$

where k_e, is a control gain and E is the overall system energy. One can observe that the input power $P_{in}(t) = F(t)\dot{x}_m(t)$ is positive when the system's energy E is below the energy target E_d and negative otherwise. The stability of the control law (67) can be proven considering $E(t)$ as a Lyapunov function candidate, as in ref. [54]. In the case of SEA, $E(t)$ can be computed as

$$E = U + K = \frac{1}{2}m_m\dot{x}_m^2 + \frac{1}{2}m_l\dot{x}_l^2 + \frac{1}{2}k(x_m - x_l)^2. \tag{68}$$

However, as the control law (67) may inject power in both the resonant and translatory modes, a slightly modified version is proposed here, to minimize the effect of temporary energy:

$$F(t) = k_e(E_d - E(t))\dot{z}_2(t) \tag{69}$$

The difference between (67) and (69) is that the latter injects energy directly on the state $\dot{z}_2$ which stores the resonant energy. Nothing prevents some energy from being injected into the state $\dot{z}_1$ as a side effect but in minor part in comparison to (67). It can be proven that the energy control law (69) implicitly acts like a damping compensation law and its stability can be proven considering $E_r(t)$, as expressed in (38), as a candidate Lyapunov function (proof is beyond the scope of this paper). Typical energy trends can be observed in Figure 8. After transients, the resonant energy E_r reaches an almost constant value, while the temporary energy E_t is still oscillating, alternating between energy accumulation and energy release phases, as expected. Power trends are reported in the lower plot where P_{in} represents the input power and $P_{dis} = P_{dis,r} + P_{dis,tB}$ the power dissipated within the system, in both resonant and nonresonant modes.

Data have been collected in 24 experiments characterized by 4 different loads, with different inertia, and with 6 different oscillation amplitudes corresponding to 6 different values for E_d in (67). Figure 9 reports the measured efficiency in comparison with the analytical expectations, including worst case

https://doi.org/10.1017/S0263574721001211 Published online by Cambridge University Press

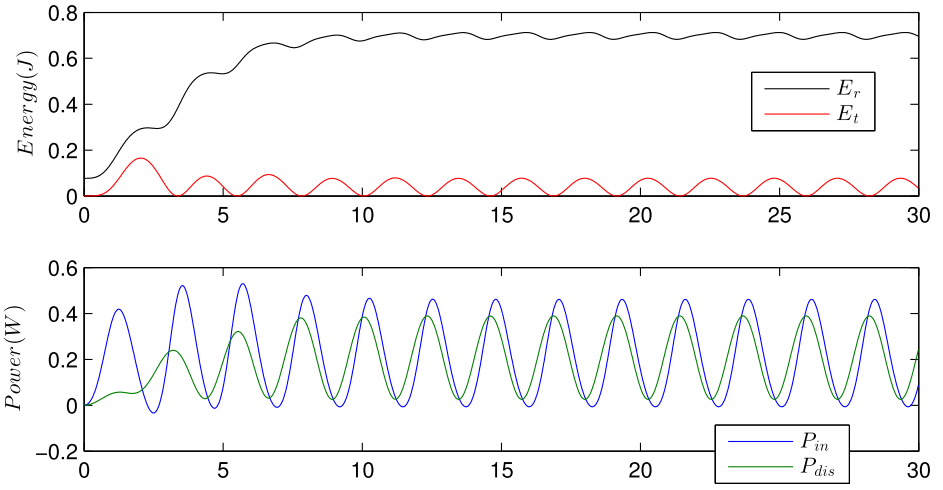


Figure 8. *Energy and power trends in SEA simulation using energy control as in (67).*

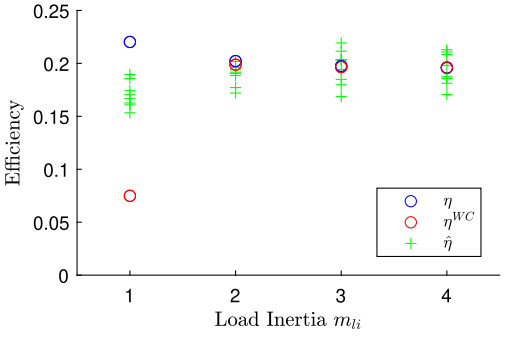


Figure 9. *SEA experimental validation: measured $\hat{\eta}$ in comparison with theoretic expectations η and η^{WC}.*

expectations as we did for the simulation results (Figures 4 and 5). The main differences in comparison with the simulation are that (1) the motor inertia is not changed, leading to a two-dimensional plot similar to those in Figure 6 instead of a three-dimensional one; (2) some noise can be observed in the measured index $\hat{\eta}$, probably due to stiction effects, shaft misalignment and cogging torques, which can influence the experimental outcome depending on the motion amplitude and on the initial experimental conditions. In particular, stiction effects may present a dynamic constraint on the load, possibly affecting the temporary energy level. In the case of higher load inertias, one can see an agreement between the measured efficiency $\hat{\eta}$ and the analytical index η. For the lowest load inertia, the index η – which neglects the temporary energy – overestimates the system efficiency which lies between η and η^{WC}, as expected. This is observed only for the lowest load inertia because this situation involves higher levels of temporary energy, in accordance with (44) and (60a).

7.3. Discussion

The results from our simulations and experiments uncover some guidelines for the efficient design of elastic actuators, which we will discuss in this section. First of all, we can state that SEAs and PEAs are characterized by different energetic behaviors. Our analysis and results show that, due to the temporary energy, SEAs are affected by additional dissipation with respect to PEAs. This is because (a) the temporary energy is not recovered and (b) the temporary energy implies additional motion, which results

https://doi.org/10.1017/S0263574721001211 Published online by Cambridge University Press

in additional dissipation. However, by simulating the SEA system considering a wide set of realistic parameter values, we found that such additional dissipation should be quite low in practice. Even in our experimental validation, we could see the effects of temporary energy only by choosing extremely low spring stiffness k and load inertia m_l. This agrees with equations (45) and (60a). However, it must be noted that higher temporary energy dissipation can show up in the case of high distal friction,, high values for d_s and d_l as shown in Figure 6. It may thus be convenient to minimize these dissipation sources. Instead, motor friction was not found to be linked to temporary energy.

Beside the dissipation due to temporary energy, some distinct characteristics of SEA and PEA efficiency can be observed. A comparison of figures 4 and 5 reveals that PEAs behave more efficiently than SEAs in some conditions. This applies in particular when the either the motor or the load inertia are high. The case of SEAs is more controversial. In particular, in the case of high dissipation in the motor, SEAs retain high efficiency only when the motor inertia is high. Similarly, in the case of high dissipation on the load, a large load inertia appears to be beneficial. This conclusion can be drawn by comparing the plots on Figures 4 and 5. So, as a general principle for SEA design, one could aim to have the higher inertia where the dissipation is higher, on the motor or on the load. Equivalently, one can prioritize the reduction of friction where the inertia is low. This does of course not mean that increasing inertia will decrease the dissipated power, which would be counterintuitive. Instead, we argue that a higher inertia makes it possible to transfer more kinetic energy which, given the same damping, leads to a longer-lasting motion.

On a final note, we would like to emphasize that energy efficiency is not the only advantage of SEAs. They also provide improved force control robustness, reduced output impedance, shock tolerance, and an additional translational mode. While PEAs can also be utilized to increase energy efficiency, they do not offer all of the aforementioned benefits.

8. Conclusions and Future Directions

This paper described an analytical energetic characterization of elastic actuators in resonant motion. It proposed an efficiency analysis which accounts for the system's internal energy as a means to normalize the dissipated power among different tasks. We highlighted the role of temporary energy and its relation to energy efficiency. We found that temporary energy causes efficiency drops due to additional dissipation and (if it cannot be recovered) negative input power. Such temporary energy arises only in the case of an SEA with "distal" dissipation sources. When accounting for temporary energy, the computation of efficiency becomes more complex and depends on load dynamics (e.g. environmental or external forces) which may be not known a priori. In those cases, the proposed analysis only considers best and worst case condition, in the knowledge that, in practice, efficiency will lie between the indices related to these two conditions. These indices are reported in Table II and in Table III.

The main objective of this paper was to demonstrate the viability of an analytical approach to characterize the efficiency of passive dynamics, independent of a specific system or task. Although the goal has been accomplished, the approach still needs to be developed further to make it practically useful. Starting from the proposed foundation, the analysis will be extended in future work to account for (i) multiple DOF systems, (ii) nonresonant motion and (i) electric dynamics and their associated losses.

Acknowledgments. This work has been partially supported by the project of the Italian Ministry of Education, Universities and Research (MIUR) "Dipartimenti di Eccellenza 2018-2022". Tom Verstraten is a postdoctoral fellow of the Research Foundation - Flanders (FWO).

References

[1] K. Kubo, Y. Kawakami and T. Fukunaga, "Influence of elastic properties of tendon structures on jump performance in humans," *J. Appl. Physiol. (Bethesda, Md. : 1985)* **87**, 2090–2096 (1999). ISSN 8750-7587.

[2] G. J. Ettema, "Mechanical efficiency and efficiency of storage and release of series elastic energy in skeletal muscle during stretch-shorten cycles," *J. Exp. Biol.* **199**, 1983–1997 (1996). ISSN 0022-0949.

https://doi.org/10.1017/S0263574721001211 Published online by Cambridge University Press

[3] T. J. Roberts, "The Integrated Function of Muscles and Tendons During Locomotion," **In:** *Comparative Biochemistry and Physiology - A Molecular and Integrative Physiology*, vol. 133 (2002) pp. 1087–1099. ISBN 1541737822. doi: 10.1016/S1095-6433(02)00244-1.

[4] G. A. Pratt and M. Williamson, "Series Elastic Actuators," **In:** *International Conference on Intelligent Robots and Systems*, vol. 1 (IEEE, 1995) pp. 399–406. http://ieeexplore.ieee.org/xpls/abs_all.jsp?arnumber=525827.

[5] A. Calanca, R. Muradore and P. Fiorini, "A review of algorithms for compliant control of stiff and fixed compliance robots, *IEEE Trans. Mechatron.* **210**(2), 613–624 (2016). doi: 10.1109/TMECH.2015.2465849.

[6] A. Calanca and P. Fiorini, "Human-adaptive control of series elastic actuators," *Robotica* **20**(08), 1301–1316 (2014). doi: 10.1017/S0263574714001519.

[7] A. Calanca and P. Fiorini, "On the Role of Compliance in Force Control," **In:** *Advances in Intelligent Systems and Computing* (E. Menegatti, N. Michael, K. Berns, and H. Yamaguchi, eds.), vol. 302, Padova, Italy (Springer International Publishing, 2016) pp. 1243–1255. doi: 10.1007/978-3-319-08338-4_90.

[8] S. Oh and K. Kong, "High precision robust force control of a series elastic actuator," *IEEE/ASME Trans. Mechatron.* **220**(1), 71–80 (2017). ISSN 1083-4435. doi: 10.1109/TMECH.2016.2614503. http://ieeexplore.ieee.org/document/7579567/.

[9] Y. Park, N. Paine and S. Oh, "Development of force observer in series elastic actuator for dynamic control," *IEEE Trans. Ind. Electron.* **00460**(c), 1–1 (2017). ISSN 0278-0046. doi: 10.1109/TIE.2017.2745457. http://ieeexplore.ieee.org/document/8016638/.

[10] E. Sariyildiz, R. Mutlu and H. Yu, "A sliding mode force and position controller synthesis for series elastic actuators," *Robotica* **380** (1), 15–28 (2020). doi: 10.1017/S0263574719000420.

[11] B. Vanderborght, B. Verrelst, R. Van Ham, M. Van Damme, D. Lefeber, B. M. Y. Duran and P. Beyl, "Exploiting natural dynamics to reduce energy consumption by controlling the compliance of soft actuators," *Int. J. Robot. Res.* **250** (4), 343–358 (2006). ISSN 0278-3649. doi: 10.1177/0278364906064566. http://ijr.sagepub.com/content/25/4/343.abstract.

[12] K. B. Albert. *Efficient Control of SEA Through Exploitation of Resonant Modes.* PhD thesis, MIT, 2007.

[13] P. Beckerle, J. Wojtusch, S. Rinderknecht and O. von Stryk. "Analysis of system dynamic influences in robotic actuators with variable stiffness," *Smart Struct. Syst.* **130** (4), 711–730 (2014). doi: 10.12989/sss.2014.13.4.711.

[14] T. Verstraten, P. Beckerle, R. Furnémont, G. Mathijssen, B. Vanderborght and D. Lefeber, "Series and parallel elastic actuation: Impact of natural dynamics on power and energy consumption," *Mech. Mach. Theory* **102**, 232–246 (2016). ISSN 0094114X. doi: 10.1016/j.mechmachtheory.2016.04.004.

[15] P. Beckerle, T. Verstraten, G. Mathijssen, R. Furnémont, B. Vanderborght and D. Lefeber, "Series and parallel elastic actuation: Influence of operating positions on design and control," *IEEE/ASME Trans. Mech.* **220**(1), 521–529 (2017). ISSN 1083-4435. doi: 10.1109/TMECH.2016.2621062.

[16] D. Paluska and H. Herr, "The effect of series elasticity on actuator power and work output: Implications for robotic and prosthetic joint design," *Robot. Autonom. Syst.* **54**, 667–673 (2006). doi: 10.1016/j.robot.2006.02.013. http://www.sciencedirect.com/science/article/pii/S0921889006000650.

[17] J. K. Hitt, T. G. Sugar, M. Holgate and R. Bellman, "An active foot-ankle prosthesis with biomechanical energy regeneration," *J. Med. Dev.* **40**(1), 011003 (2010). doi: 10.1115/1.4001139.

[18] D. F. B. Haeufle, M. D. Taylor, S. Schmitt and H. Geyer, "A Clutched Parallel Elastic Actuator Concept: Towards Energy Efficient Powered Legs in Prosthetics and Robotics," **In:** 2012 *4th IEEE RAS EMBS International Conference on* Biomedical Robotics and Biomechatronics (BioRob), (June 2012) pp. 1614–1619. doi: 10.1109/BioRob.2012.6290722. http://ieeexplore.ieee.org/lpdocs/epic03/wrapper.htm?arnumber=5628015.

[19] T. Verstraten, L. Flynn, J. Geeroms, B. Vanderborght and D. Lefeber, "On the Electrical Energy Consumption of Active Ankle Prostheses with Series and Parallel Elastic Elements," **In:** 2018 *7th IEEE International Conference on Biomedical Robotics and Biomechatronics (BioRob)* (2018) pp. 720–725. doi: 10.1109/BIOROB.2018.8487656.

[20] R. Blickhan, *The Spring-Mass Model for Running and Hopping* (1989). ISSN 00219290.

[21] T. McGeer, "Passive dynamic walking," *Int. J. Robot. Res.* **9**, 62–82 (1990). ISSN 0278-3649. doi: 10.1177/027836499000900206.

[22] T. G. Sugar, K. W. Hollander, A. Boehler and J. Ward, "Comparison and analysis of a robotic tendon and jackspring actuator for wearable robotic systems," *J. Med. Dev.* **70**(4), 41003 (2013).

[23] J. A. Ward, T. G. Sugar and K. W. Hollander, "Using the Translational Potential Energy of Springs for Prosthetic systems," **In:** *2011 IEEE International Conference on Control Applications (CCA)*. (IEEE, 2011) pp. 1461–1467.

[24] S. Wang, W. van Dijk and H. van der Kooij, "Spring Uses in Exoskeleton Actuation Design," **In:** *IEEE International Conference on Rehabilitation Robotics*, vol. 2011 (2011). ISBN 9781424498628. doi: 10.1109/ICORR.2011.5975471. http://www.ncbi.nlm.nih.gov/pubmed/22275669.

[25] F. L. Moro, N. G. Tsagarakis and D. G. Caldwell, "Walking in the resonance with the COMAN robot with trajectories based on human kinematic motion primitives (kMPs)," *Autonom. Robots* **360**(4), 331–347 (2013). ISSN 0929-5593. doi: 10.1007/s10514-013-9357-9. http://link.springer.com/10.1007/s10514-013-9357-9.

[26] P. Kormushev, B. Ugurlu, S. Calinon, N. G. Tsagarakis and D. G. Caldwell, "Bipedal Walking Energy Minimization by Reinforcement Learning with Evolving Policy Parameterization," **In:** *2011 IEEE/RSJ International Conference on Intelligent Robots and Systems* (2011) pp. 318–324. doi: 10.1109/IROS.2011.6094427. http://ieeexplore.ieee.org/lpdocs/epic03/wrapper.htm?arnumber=6094427.

[27] L. Flynn, J. Geeroms, R. Jimenez-Fabian, B. Vanderborght, N. Vitiello and D. Lefeber, "Ankle-knee prosthesis with active ankle and energy transfer: Development of the CYBERLEGs Alpha-Prosthesis," *Robot. Autonom. Syst.* (2014). ISSN 09218890. doi: 10.1016/j.robot.2014.12.013. http://www.sciencedirect.com/science/article/pii/S0921889014003108.

https://doi.org/10.1017/S0263574721001211 Published online by Cambridge University Press

[28] M. Uemura and S. Kawamura, "Resonance-Based Motion Control Method for Multi-Joint Robot Through Combining Stiffness Adaptation and Iterative Learning Control," **In:** *2009 IEEE International Conference on Robotics and Automation* (2009) pp. 1543–1548. doi: 10.1109/ROBOT.2009.5152717. http://ieeexplore.ieee.org/lpdocs/epic03/wrapper.htm?arnumber=5152717.

[29] H. Goya, K. Matsusaka, M. Uemura, Y. Nishioka and S. Kawamura, "Realization of High-Energy Efficient Pick-and-Place Tasks of SCARA Robots by Resonance," **In:** *2012 IEEE/RSJ International Conference on Intelligent Robots and Systems* (2012) pp. 2730–2735. doi: 10.1109/IROS.2012.6386084. http://ieeexplore.ieee.org/lpdocs/epic03/wrapper.htm?arnumber=6386084.

[30] B. Vanderborght, A. Albu-Schaeffer, A. Bicchi, E. Burdet, D. Caldwell, R. Carloni, M. Catalano, O. Eiberger, W. Friedl, G. Ganesh, M. Garabini, M. Grebenstein, G. Grioli, S. Haddadin, H. Hoppner, A. Jafari, M. Laffranchi, D. Lefeber, F. Petit, S. Stramigioli, N. Tsagarakis, M. Van Damme, R. Van Ham, L. Visser and S. Wolf, "Variable impedance actuators: A review," *Robot. Autonom. Syst.* (2013). ISSN 09218890. doi: 10.1016/j.robot.2013.06.009. http://linkinghub.elsevier.com/retrieve/pii/S0921889013001188.

[31] J. Hitt, T. Sugar, M. Holgate, R. Bellman and K. Hollander, "Robotic transtibial prosthesis with biomechanical energy regeneration," *Ind. Robot Int. J.* **360**(5), 441–447 (2009). ISSN 0143-991X. doi: 10.1108/01439910910980169. https://doi.org/10.1108/01439910910980169.

[32] A. van den Bogert, "Exotendons for assistance of human locomotion," *Biomed. Eng. Online* **20**(1), 17–24 (2003). http://www.biomedcentral.com/content/pdf/1475-925X-2-17.pdf.

[33] J. Ortiz, T. Poliero, G. Cairoli, E. Graf and D. G. Caldwell, "Energy efficiency analysis and design optimization of an actuation system in a soft modular lower limb exoskeleton," *IEEE Robot. Automat. Lett.* **30**(1), 484–491 (2018). ISSN 2377-3766. doi: 10.1109/LRA.2017.2768119.

[34] T. Bacek, M. Moltedo, C. Rodriguez-Guerrero, J. Geeroms, B. Vanderborght and D. Lefeber, "Design and evaluation of a torque-controllable knee joint actuator with adjustable series compliance and parallel elasticity," *Mech. Mach. Theory* **130**, 71–85 (2018). ISSN 0094-114X. doi: https://doi.org/10.1016/j.mechmachtheory.2018.08.014. https://www.sciencedirect.com/science/article/pii/S0094114X18307559.

[35] M. Grimmer, M. Eslamy and A. Seyfarth, "Energetic and peak power advantages of series elastic actuators in an actuated prosthetic leg for walking and running," *Actuators* **30**(1), 1–19 (2014). ISSN 2076-0825. doi: 10.3390/act3010001. http://www.mdpi.com/2076-0825/3/1/1/.

[36] M. Eslamy, M. Grimmer and A. Seyfarth, "Adding Passive Biarticular Spring to Active Mono-articular Foot Prosthesis: Effects on Power and Energy Requirement," **In:** *IEEE-RAS International Conference on Humanoid Robots (Humanoids)*, Madrid, Spain (2014) pp. 677–684. ISBN 9781479971732.

[37] E. Bolívar, S. Rezazadeh, T. Summers and R. D. Gregg, "Robust Optimal Design of Energy Efficient Series Elastic Actuators: Application to a Powered Prosthetic Ankle," **In:** *2019 IEEE 16th International Conference on Rehabilitation Robotics (ICORR)* (2019) pp. 740–747. doi: 10.1109/ICORR.2019.8779446.

[38] A. Kamadan, G. Kiziltas and V. Patoglu, A systematic design selection methodology for system-optimal compliant actuation," *Robotica* **370**(4), 656–674 (2019). doi: 10.1017/S0263574718001248.

[39] A. G. Gonzalez-Rodriguez, A. Gonzalez-Rodriguez and F. Castillo-Garcia, "Improving the energy efficiency and speed of walking robots," *Mechatronics* **240**(5), 476–488 (2014). ISSN 0957-4158. doi: https://doi.org/10.1016/j.mechatronics.2014.05.004.

[40] A. Mazumdar, S. J. Spencer, C. Hobart, J. Salton, M. Quigley, T. Wu, S. Bertrand, J. Pratt and S. P. Buerger, Parallel elastic elements improve energy efficiency on the STEPPR bipedal walking robot, *IEEE/ASME Trans. Mechatron.* **220**(2), 898–908 (2017). ISSN 1941-014X. doi: 10.1109/TMECH.2016.2631170.

[41] J. Reher, E. A. Cousineau, A. Hereid, C. M. Hubicki and A. D. Ames, "Realizing Dynamic and Efficient Bipedal Locomotion on the Humanoid Robot Durus," **In:** *2016 IEEE International Conference on Robotics and Automation (ICRA)* (2016) pp. 1794–1801. doi: 10.1109/ICRA.2016.7487325.

[42] H. Q. Vu, X. Yu, F. Iida and R. Pfeifer, "Improving energy efficiency of hopping locomotion by using a variable stiffness actuator," *IEEE/ASME Trans. Mechatron.* **210**(1), 472–486 (2016). ISSN 1083-4435. doi: 10.1109/TMECH.2015.2428274.

[43] Y. Yesilevskiy, Z. Gan and C. D. Remy, *Optimal configuration of series and parallel elasticity in a 2D monoped* (2016).

[44] X. Liu, A. Rossi and I. Poulakakis, "A switchable parallel elastic actuator and its application to leg design for running robots," *IEEE/ASME Trans. Mechatron.* **230**(6), 2681–2692 (2018). doi: 10.1109/TMECH.2018.2871670.

[45] M. Scheint, M. Sobotka and M. Buss, "Optimized Parallel Joint Springs in Dynamic Motion: Comparison of Simulation and Experiment," **In:** *2010 3rd IEEE RAS & EMBS International Conference on Biomedical Robotics and Biomechatronics* (2010) pp. 485–490. doi: 10.1109/BIOROB.2010.5628015.

[46] N. Schmit and M. Okada, "Optimal design of nonlinear springs in robot mechanism: simultaneous design of trajectory and spring force profiles," *Adv. Robot.* **270**(1), 33–46 (2013). doi: 10.1080/01691864.2013.751162. https://doi.org/10.1080/01691864.2013.751162.

[47] R. Nasiri, M. Khoramshahi, M. Shushtari and M. N. Ahmadabadi, "Adaptation in variable parallel compliance: Towards energy efficiency in cyclic tasks," *IEEE/ASME Trans. Mechatron.* **220**(2), 1059–1070 (2017). ISSN 1083-4435. doi: 10.1109/TMECH.2016.2637826.

[48] M. Shushtari, R. Nasiri, M. J. Yazdanpanah and M. N. Ahmadabadi, Compliance and frequency optimization for energy efficiency in cyclic tasks, *Robotica* **350**(12), 2363–2380 (2017). doi: 10.1017/S0263574717000030.

[49] F. Valero, F. Rubio and C. Llopis-Albert, "Assessment of the effect of energy consumption on trajectory improvement for a car-like robot," *Robotica* **370**(11), 1998–2009 (2019). ISSN 14698668. doi: 10.1017/S0263574719000407.

https://doi.org/10.1017/S0263574721001211 Published online by Cambridge University Press

[50] B. Vanderborght, R. VanHam, D. Lefeber, T. G. Sugar and K. W. Hollander, "Comparison of mechanical design and energy consumption of adaptable, passive-compliant actuators," *Int. J. Robot. Res.* **280**(1), 90–103 (2009). ISSN 0278-3649. doi: 10.1177/0278364908095333. http://ijr.sagepub.com/cgi/doi/10.1177/0278364908095333.
[51] S. Teitler and R. Proodian, "What price speed", revisited (1980). ISSN 0146-0412.
[52] W. Shi, D. Stapersma and H. T. Grimmelius, "Comparison study on moving and transportation performance of transportation modes," *Int. J. Energy Environ.* **20**(4), 179–190 (2008).
[53] A. Calanca, L. M. Capisani, A. Ferrara and L. Magnani, "MIMO closed loop identification of an industrial robot," *IEEE Trans. Cont. Syst. Technol.* **190**(5), 1214–1224 (2011). ISSN 1063-6536. doi: 10.1109/TCST.2010.2077294. http://ieeexplore.ieee.org/xpls/abs_all.jsp?arnumber=5634145http://ieeexplore.ieee.org/lpdocs/epic03/wrapper.htm?arnumber=5634145.
[54] M. Spong and G. Bhatia, "Further Results on Control of the Compass Gait Biped," **In:** *Proceedings 2003 IEEE/RSJ International Conference on Intelligent Robots and Systems (IROS 2003) (Cat. No.03CH37453)*, vol. 2 (IEEE, 2003) pp. 1933–1938. ISBN 0-7803-7860-1. doi: 10.1109/IROS.2003.1248927.

Cite this article: A. Calanca and T. Verstraten (2022). "An energy efficiency index for elastic actuators during resonant motion", Robotica **40**, 1450–1474. https://doi.org/10.1017/S0263574721001211

https://doi.org/10.1017/S0263574721001211 Published online by Cambridge University Press